Paper No.
04077

CORROSION2004

COOLING WATER MONITORING USING COUPLED MULTIELECTRODE ARRAY SENSORS AND OTHER ON-LINE TOOLS

Michael H. Dorsey
DuPont Engineering Technology
Orange, Texas 77630, USA

Lietai Yang and Narasi Sridhar
Southwest Research Institute
San Antonio, TX 78238–5166, USA

ABSTRACT

Real-time coupled multielectrode array sensors (MAS) and other monitoring tools were used to evaluate a complex corrosion phenomenon on carbon steel in a large industrial cooling water system. The design and implementation of the monitoring system, and monitoring results are discussed in this paper. Characterization of the degree and depth of attack from the MAS probe showed excellent correlation with characterization of underdeposit attack on corrosion coupons that were exposed simultaneously with the MAS probe.

INTRODUCTION

Fresh pond water was used for cooling process equipment in a large DuPont chemical plant. The cooling water system operates in a closed recirculating mode and circulates approximately 1/3 of the pond's volume (140 MM gallon) through each day. Localized corrosion has been observed in coupon and microbiological testing [1]. As the water contains high levels of biological activity, the observed localized corrosion may be attributed to microbiologically influenced corrosion.

To understand the occurrence of localized corrosion, and its relationship to microbiological induced corrosion, coupled multielectrode array sensors and other on-line monitoring tools were installed in side loops of a testing station in the cooling water system. This paper reports the preliminary results.

EXPERIMENTAL

Test Loop

There are two loops in the testing station, one from the outlet of the cooling water system, and the other from the incoming or makeup water . Online sensors were installed in both the outlet loop and the makeup water loop. Figure 1 shows the test loops.

Coupled Multielectrode Array Sensors

The coupled multielectrode array sensor and the high-resolution monitoring system have been described elsewhere [2,3]. Figure 2 shows typical coupled multielectrode array sensor probes for application in cooling systems. In Figure 2, the sensing electrodes are coupled to simulate one piece of a metal, with some electrodes acting as anodic sites and other electrodes acting as cathodic sites. Each anodic coupling current represents the degree of charge transfer from a corroding (or more corroding) site to a non-corroding (or less corroding) site, which is part of the non-uniform corrosion process. Therefore the currents that flow from the anodes (or more anodic electrodes) to the cathodes (or less anodic electrodes) are measured as the corrosion signal.

Three sensors designated as CS-E4, CS-E5, and CS-E6 were used in the test. Sensors CS-E4 and CS-E6 were placed in the outlet loop and sensor CS-E5 was placed in the makeup water loop. The sensing electrodes of sensors CS-E4 and E5 were made of 1.21-mm-diameter Type 1008 carbon steel (UNS G10080) wire; the sensing electrodes of sensor CS-E6 were made of 1.0-mm-diameter Type 1010 carbon steel (UNS G10010) wire. The compositions of the two types of carbon steel wires are given in Table 1. As the two types of wires were close in composition, no difference in corrosion rate was expected between the two types of wires. All sensors were built with 24 sensing electrodes that were cast in epoxy, and only the cross section at the sensor tip was exposed to the process solution. The electrode areas were 0.0115 cm^2 for sensors CS-E4 and CS-E5, and 0.00785 cm^2 for sensor CS-E6. Prior to the test, the sensing surface of the sensors (the tip of the sensor) was polished with 600-grit paper and cleaned with acetone. All sensing surfaces of the probes were installed facing the flow in the test loops.

A calomel reference electrode was installed in the outlet water loop in close proximity to sensors CS-E4 and CS-E6 for the measurements of the coupling potentials of the sensors.

RESULTS AND DISCUSSIONS

Figures 3 and 4 show the current density signals from sensor CS-E5 that was installed in the makeup water loop and the average signals from sensors CS-E4 and CS-E6, both of which were installed in the outlet water loop. Sensors CS-E4 and CS-E5 were installed at the beginning of the test and sensor CS-E6 was installed two months later. The signals in Figure 3 were represented by three times the standard deviation values, and the signals in Figure 4 were represented by the maximum anodic current densities of the currents from the 24 electrodes in each sensor. Both representations were used in previous studies[3].

The 24 mini-electrodes in each sensor simulate a test coupon that is divided into 24 areas, and the most anodic current density from the 24 mini-electrodes in each sensor as shown in Figure 3 simulates the corrosion rate of the most corroding area in a coupon. Because a real coupon may develop hundreds of pits in a corrosive environment, the use

of a three times standard deviation signal is a way to estimate the most anodic current density based on a statistical approach and, thus, is considered more reliable[3]. Figures 3 and 4 show that the two signals are close to each other and they can be used interchangeably as the corrosion signal of the sensors under the testing conditions.

Apparent corrosion rate may be obtained using Faraday's law by assuming that the corrosion on the most corroded mini-electrode was corroded uniformly. This is a reasonable approach because the surface area of each sensing electrode in the sensors are small (approximately 10^4 times less than that in a typical linear polarization (LPR) probe or an electrochemical noise probe). Figure 5 shows the apparent localized corrosion penetration rates for the mild carbon steel sensors based on the most anodic current densities in the two test loops during the 5.5-month monitoring period. Each of these rates corresponds to the pitting rate at the most active area of a test coupon.

The initial corrosion penetration rate in the makeup water was exceptionally high at approximately 12 mm/year or 472 mil/year at the beginning of the measurements. The signal decreased two weeks later and stabilized at approximately 1.2 mm/year or 47 mil/year near the end of the measurements. The exceptionally high penetration rate observed during the start of the measurements may be attributed to the fresh surface of the electrodes. Once the electrode corroded, the rate decreased because the corrosion product formed a diffusion layer on the metal and limited the corrosion rate. A general trend for the corrosion rate observed in the makeup water was that the rate was high during the start (not accounting for the data in the first three weeks) and lower at the end of the measurements. This trend is could be due to the temperature change in the ponds that were warm in the fall and colder in the winter (Figure 3) because this water was not heated or cooled before reaching the test station. There were several sudden increases and decreases in the corrosion signals from the probe, some of which may be attributed to sudden flow changes. A sudden restart of the flow after a few days shut down may cause spalling of the corrosion products on the surface of the sensor and result in a higher short-term corrosion rate. The average penetration rate which corresponds to the rate at the most active pitting area of a coupon over the 5.5-month monitoring period was 3.78 mm/year (149 mil/year).

Unlike the case in the makeup loop, the trend of the corrosion rate in the outlet water is not so consistent because the temperature was less affected by the weather and there were more changes in the variables that might affect corrosion. These variables include corrosion inhibitor, pH, conductivity and dissolved oxygen. Because of the changes in many process variables, the measured corrosion rate which corresponds to the rate at the most active pitting area of a test coupon in the Outlet water system fluctuated between 0.2 to 7.5 mm/year (7.87 to 295 mil/year). The increase in sensor CS-E4's signal on 10/14/02 was due to a flow surge when the valve to the loop was re-opened. The average penetration rate for the most active pitting area over the 5.5-month monitoring period in the outlet water was 2.67 mm/year (105 mil/year).

Figure 6 also shows the signals from the outlet water at the beginning and at the end of the monitoring period are essentially the same, indicating that the sensor worked well

in the cooling water system for 5.5 months without the need to be re-conditioned. At the end of the 5.5-month period, the sensors were taken out for post-test examination.

Figure 7 shows that patches of thick and loose deposits were typically formed on the sensing surfaces of the sensors after in the cooling water system for 5.5 months. Figure 8 shows typical post-service appearance of the sensing electrodes after removal of the deposits. Some of the electrodes were severely corroded and others were less corroded. During the measurements, the severely corroded electrodes acted as the anodes and the less corroded electrodes acted as the cathodes. The depth of attack of the most corroded electrode (measured after removal of the deposits) was 34 mil for sensor CS-E4 and 54 mil for sensor CS-E6. Sensor CS-E4 was in service for 5.5 months and sensor CS-E6 was in service for 3 months. The converted yearly penetration rates are 1.88 mm/year (74 mil/year) for the most active electrode in sensor CS-E4 and 5.48 mm/year (216 mil/year) for the most active electrode in sensor CS-E6. The average penetration rate from the two sensors is 3.68 mm/year (145 mil/year) which is surprisingly close to the measured average rate as shown in Figure 5 for the outlet water (3.78 mm/year or 149 mil/year).

The sensors were re-installed in their previous locations after the sensing electrodes were examined and cleaned with 200-grit paper. Figure 9 shows the measured localized corrosion penetration rates that were derived from the most anodic current densities of the three sensors for another 16-day period. Similar to the signal from the makeup water as shown in Figure 5, all the signals increased following the start of the measurements and reached their maximum values in about 10 days. (All signals seemed to be on the decrease trend near the end of the test two weeks after the start). Figure 9 also shows that the two sensors (CS-E4 and CS-E6) fluctuated similarly, indicating that the fluctuations were due to the effect of the process parameters such as temperature, pH, flow rate or inhibitor concentrations. The localized corrosion signal from the sensor in the makeup water seems to be lower than those from the sensors in the outlet water system. This may be due to the fact that the outlet water temperature was higher than that of the makeup water during this period.

Figure 10 shows the potentials measured from the coupling joints of the two sensors in the return water system. The potential of the CS-E4 sensor was higher than that of the CS-E6 sensor, indicating CS-E6 was undergoing more localized corrosion. This is in agreement with the measured localized corrosion rates as shown in Figure 9. Figure 10 also shows a decreasing trend for the sensor potentials during the measurement period, indicating an increase in localized corrosion signals. This is indeed in agreement with the measured results shown in Figure 9.

Figure 11 shows typical post-test appearances of the sensor before and after removing the loose deposits. The electrodes under the deposits were severely corroded and the electrodes not covered by the deposits were not corroded after the 16-day exposure in the cooling water system. This large difference in degree of attack is typical of microbiologically influenced corrosion[4]. The corroded electrodes were likely the anodes and the unattacked electrodes were more likely the cathodes. Figure 12, which shows typical currents from each electrode of a sensor, indicates that a significant

number of the electrodes were anodes (negative currents) and the rests were cathodes (positive currents).

The deposits on the sensors removed after the 16-day-monitoring period were analyzed using energy dispersive spectroscopy (EDS). Table 2 shows the EDS results for a sensor from the return water loop (CS-E4) and a sensor from the makeup water loop (CS-E5). Compared with the composition of the sensing electrodes (Table 1), the deposits contained significant amount of P, Si, S and Ca. In addition, the deposit on the sensor in the return water contains more P, Si, Al and Ca, but less Cu than that in the makeup water. The sulfur content may be an indication the presence of sulfate reducing bacteria (SRB) in the cooling water. The presence of bacteria in the corrosion products were also confirmed by DNA analyses to consist of a significant amount of SRB as well as IRB (iron reducing bacteria). In addition, weekly sessile counts of bacteria levels in the water were performed as well as use of HACH test kits for SRB and IRB showed positve results confirming indication of bacteria.

Corrosion coupons were also exposed on a monthly basis. The overall corrosion rates that were calculated on the basis of weight loss showed rates that were in the range of 15-30 mpy over this time period, with an average rate of about 20 mpy. However, it should be noted that these corrosion rates are actually misleading because they did not truly reflect the rate of non-uniform under deposit corrosion that was actually occurring under the deposits that consistently built up on the samples as was shown in Figure 7. Figure 13 illustrates the degree of non-uniform corrosion on a cleaned corrosion coupon. Note that the areas outside of the under-deposit corroded locations still show the machining lines of the coupons from fabrication suggesting that once under-deposit corrosion initiated, corrosion propagated rapidly in these areas. Infact, measurements of depth of attack in these under-deposit corroded areas showed depths of attack that were 5-10X of the general corrosion rates, which translates to localized under-deposit corrosion rates of 100-200 mpy.

It is interesting to note that the “under-deposit” corrosion rates of 100-200 mpy were consistent with the average penetration rates of 100-150 mpy that were measured by the MAS probe. In addition, the areas outside the corroded areas of the coupons were relatively unattacked which was manifested in the MAS probes where a number of the electrodes were unattacked, and others were significantly attacked. This suggests that the design of the MAS probe with small and independent electrodes on the surface can truly simulate the non-uniform and random incidences of underdeposit corrosion on the coupons.

CONCLUSIONS

The system has experienced severe localized and under deposit corrosion on carbon steel that continues to impact the integrity of carbon steel equipment and other metallurgy. There was excellent correlation between the experimentally determined pitting penetration rates on the electrodes with the depths of attack measured on both the electrodes as well as the corrosion coupons. In addition, the dominant and preferential attack on a few of the sensors of the probe (anodic sites) versus the rest of the sensors that were unattacked (cathodic sites) was consistent with the non uniform and under deposit corrosion that was observed on the coupons. Both these correlations of depths of attack and the similarities in the degree of attack confirms that the MAS probe effectively simulated the localized corrosion of steel in this system, and the current signals were a reasonable reflection of anodic and cathodic sites that are randomly generated on different areas of a metal surface.

ACKNOWLEDGMENTS

The authors acknowledge the assistance of Dan Demarco and Brian Saldanha (both from DuPont Co.), for their technical input and data data analysis, and of Kevin Daigle (Chemtreat Co.) for his assistance in providing some of the water chemistry data.

.

REFERENCES

1. Michael H. Dorsey, George J. Licina, Brian J. Saldanha and Richard C. Ebersole, "Monitoring for Corrosion and Microbiological Activity in a Cooling Water System", CORROSION/2002, paper no. 02009, (Houston, TX: NACE International, 2002).

2. Lietai Yang and Narasi Sridhar "Coupled Multielectrode Online Corrosion Sensor", Materials Performance, September, p (2003).

3. L. Yang, N. Sridhar, O. Pensado, and D. S. Dunn, "An In-situ Galvanically Coupled Multielectrode Array Sensor for Localized Corrosion", Corrosion, 58, 1004, 2002.

4. D. Thierry and W. Sand, "Microbially Influenced Corrosion", in Corrosion Mechanisms in Theory and Practice, P. Marcus and J. Oudar Eds, Marcel Dekker, Inc., 1995, New York, Chapter 13, page 457.

5. P. Marcus, "Sulfur-assisted Corrosion Mechanisms and the Role of Alloyed Elements", in Corrosion Mechanisms in Theory and Practice, P. Marcus and J. Oudar eds., Marcel Dekker, inc., New York, 1995, page 239.

Table 1.
Chemical compositions (wt %) of the metal wires used in the sensors

Metals	UNS #	Fe	Mn	P	S	C
1010 CS	G10100	Bal	0.31	0.04	0.042	0.08
1008 CS	G10080	Bal	0.40	0.04	0.042	0.1

Table 2
EDS analysis results for the loose deposits on the sensors

Sensor	Fe	P	Si	S	Cu	Al	Ca	Mn	Cl
Deposits on CS-E4, used in return water	78.82	13.58	3.06	1.14	-	1.16	1.74	-	0.5
Deposits on CS-E5, used in makeup water	86.22	5.56	2.31	1.54	1.27	0.61	0.76	0.56	0.32

Figure 1: **Field Test loop for exposure of Multielectrode Array Sensor Probe and Corrosion Coupons**

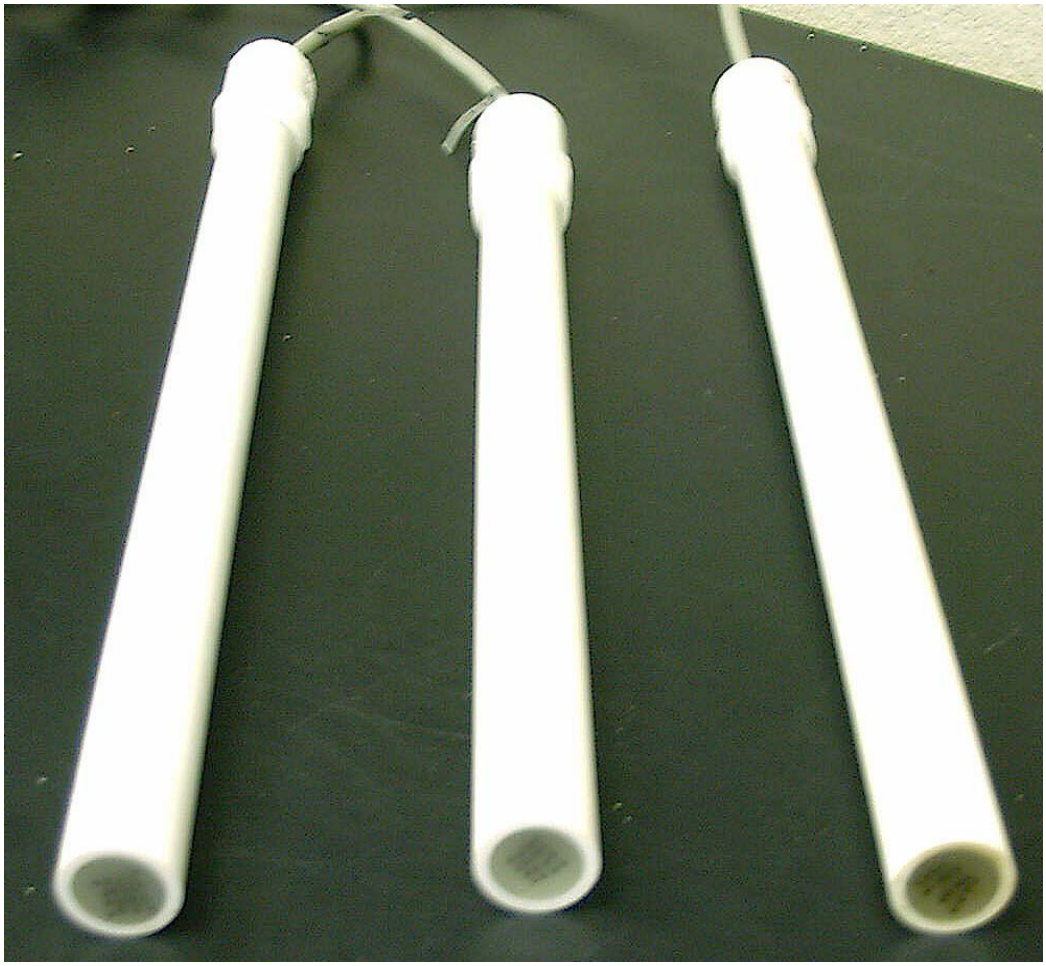

Figure 2: Typical coupled multielectrode array sensor probes for application in cooling systems

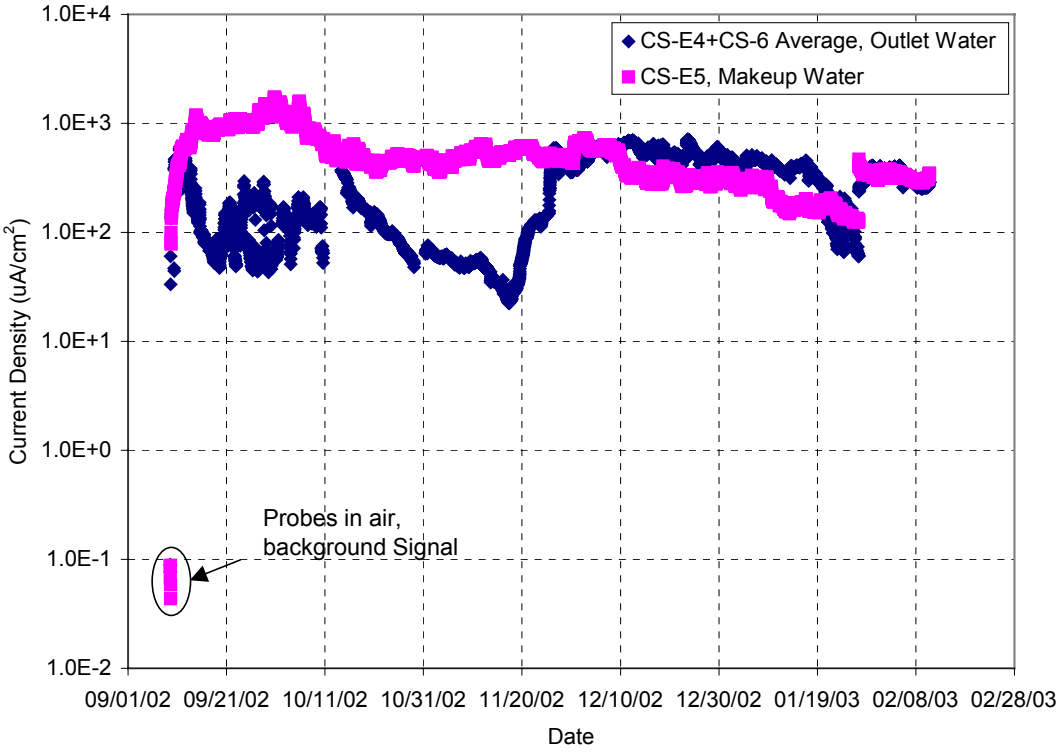

Figure 3: **Localized corrosion signals as represented by three times standard deviation of current densities from the different electrodes of the sensors in the two loops.**

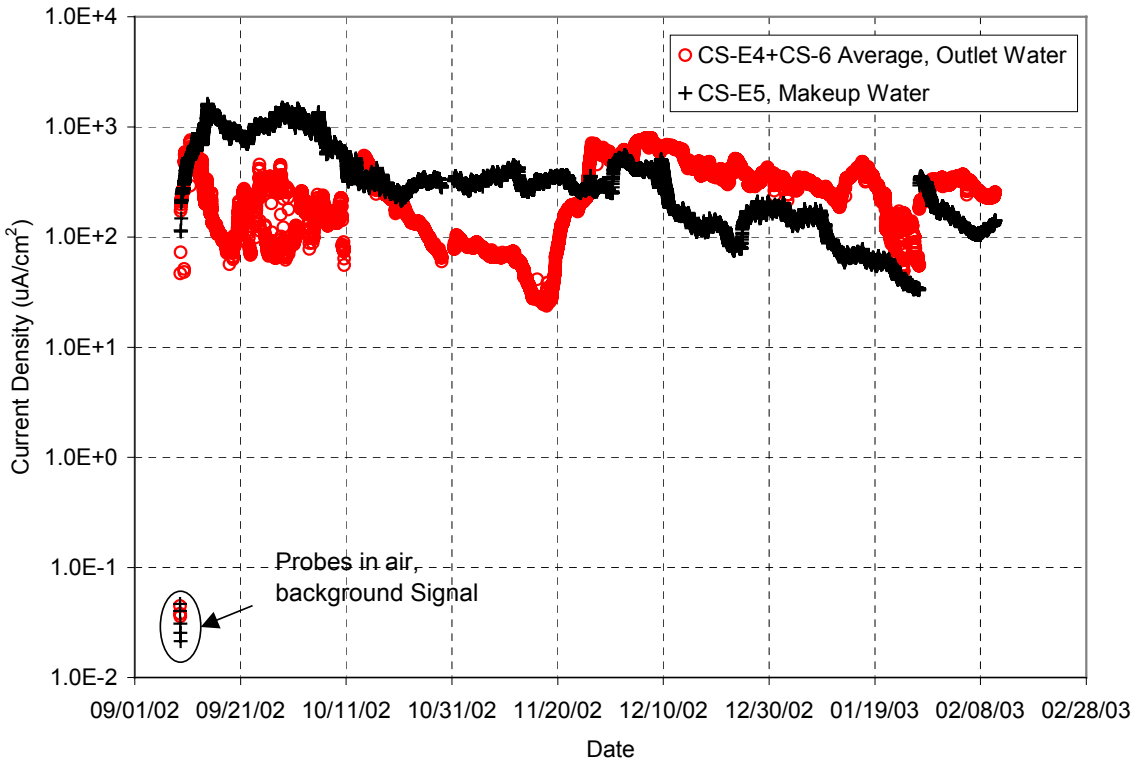

Figure 4: **Localized corrosion signals as represented by the maximum anodic current densities from the different electrodes of the sensors in the two loops.**

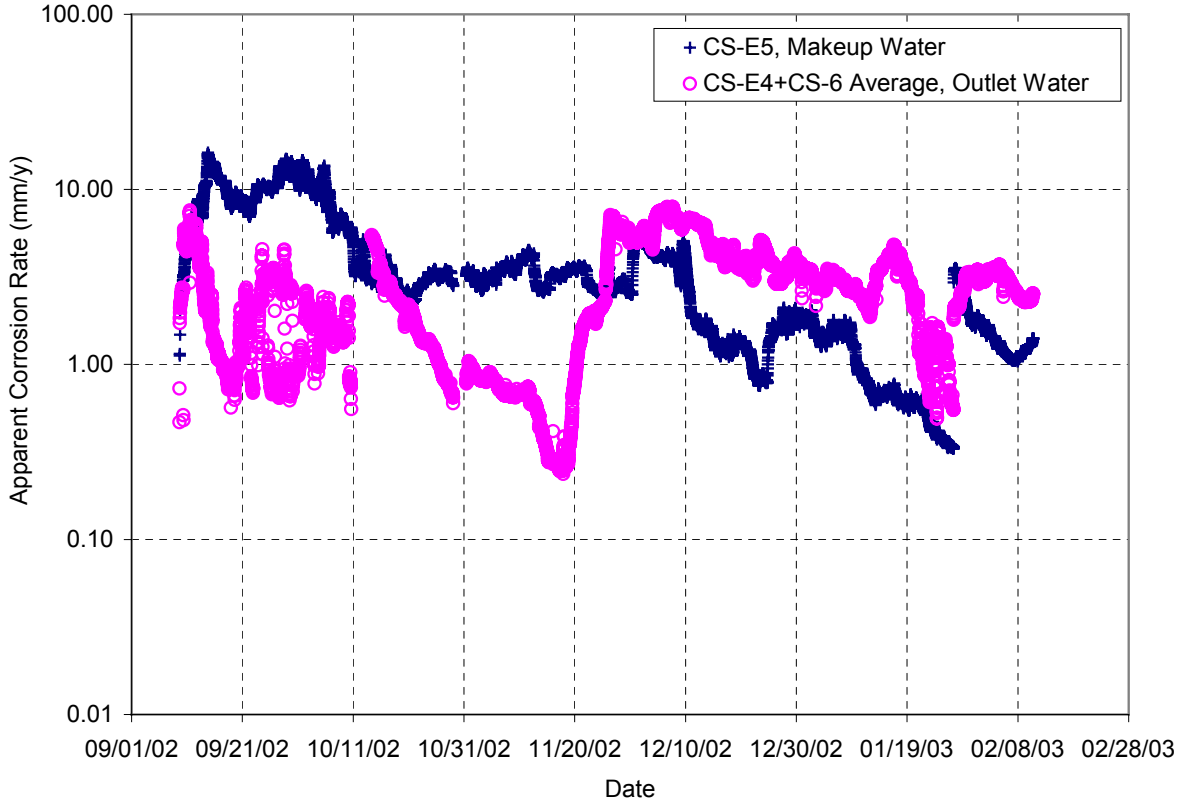

Figure 5: **Apparent localized corrosion penetration rates based on maximum anodic current densities from the different electrodes of the sensors in the two loops.**

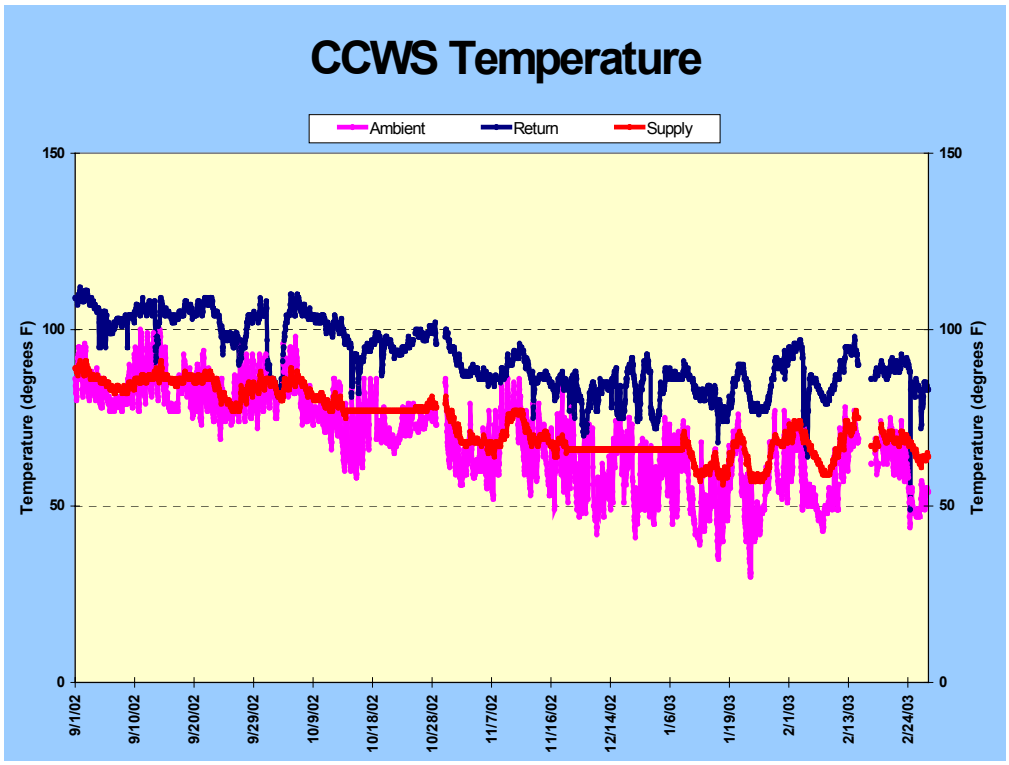

Figure 6: **Temperature of the Make-Up Water – "Supply" represents the inlet or "make-up" water, and "Return" represents the outlet water.**

Figure 7: **Typical appearance of deposits formed on the surface of the sensors after 5.5-months in the cooling water system. Note: A-front view; B- side view; the deposits was approximately 5 mm thick.**

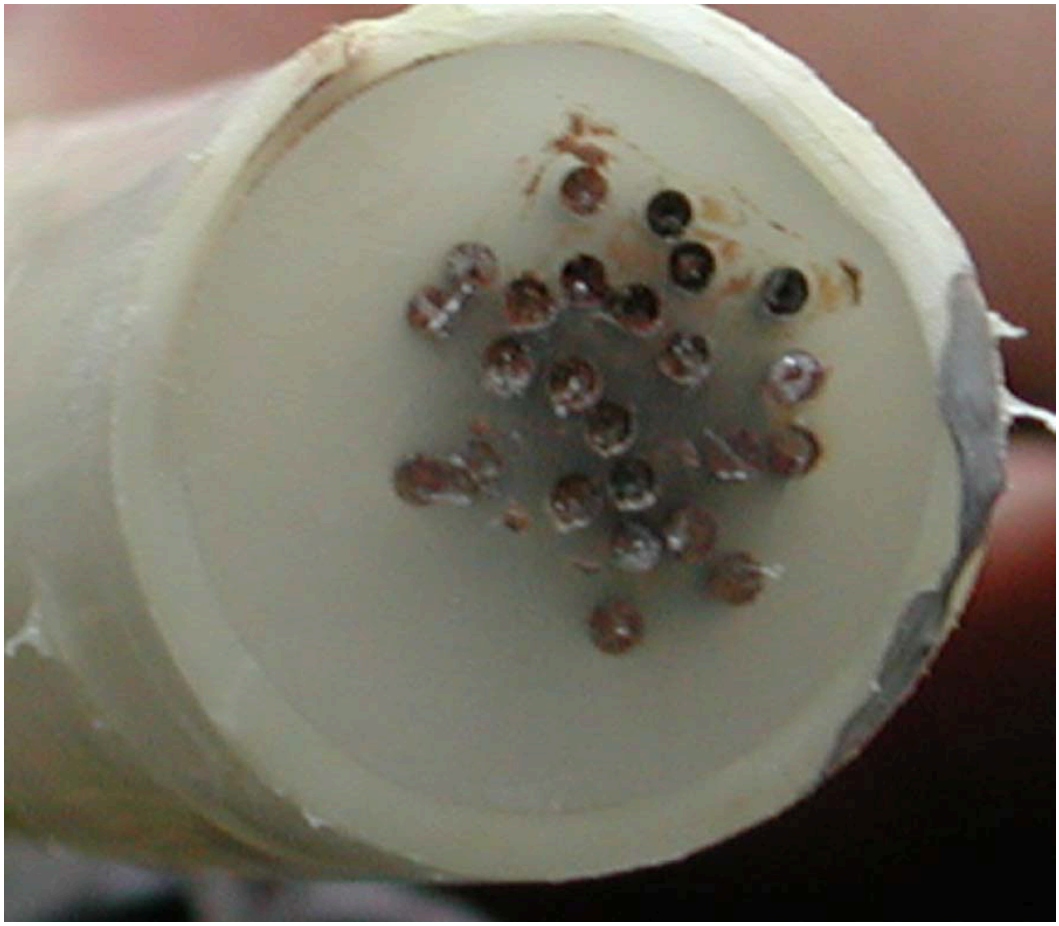

Figure 8: **Typical post-service appearance of the sensing surface after the removal of the loose deposits. Some sensing electrodes were severely corroded**

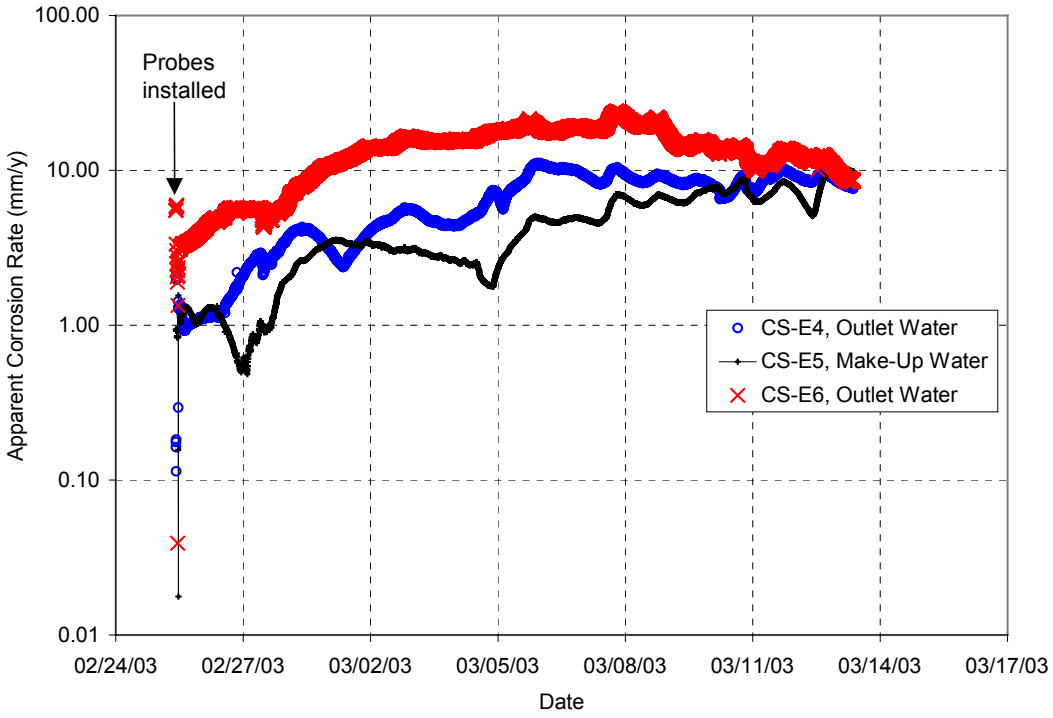

Figure 9: **Apparent localize corrosion pennetration rates from the three sensors installed in the cooling water system during a shot-term**

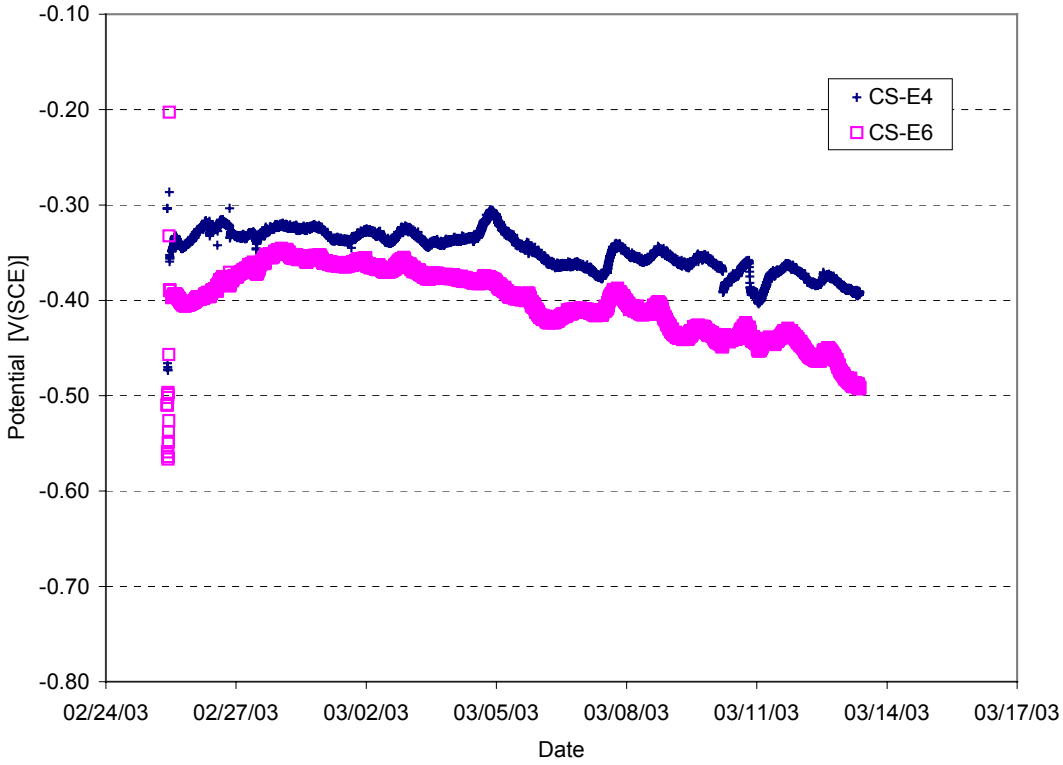

Figure 10: Electrochemcial potentials of the two carbon steel probes in the outlet water loop during the measurements shown in Figure 9.

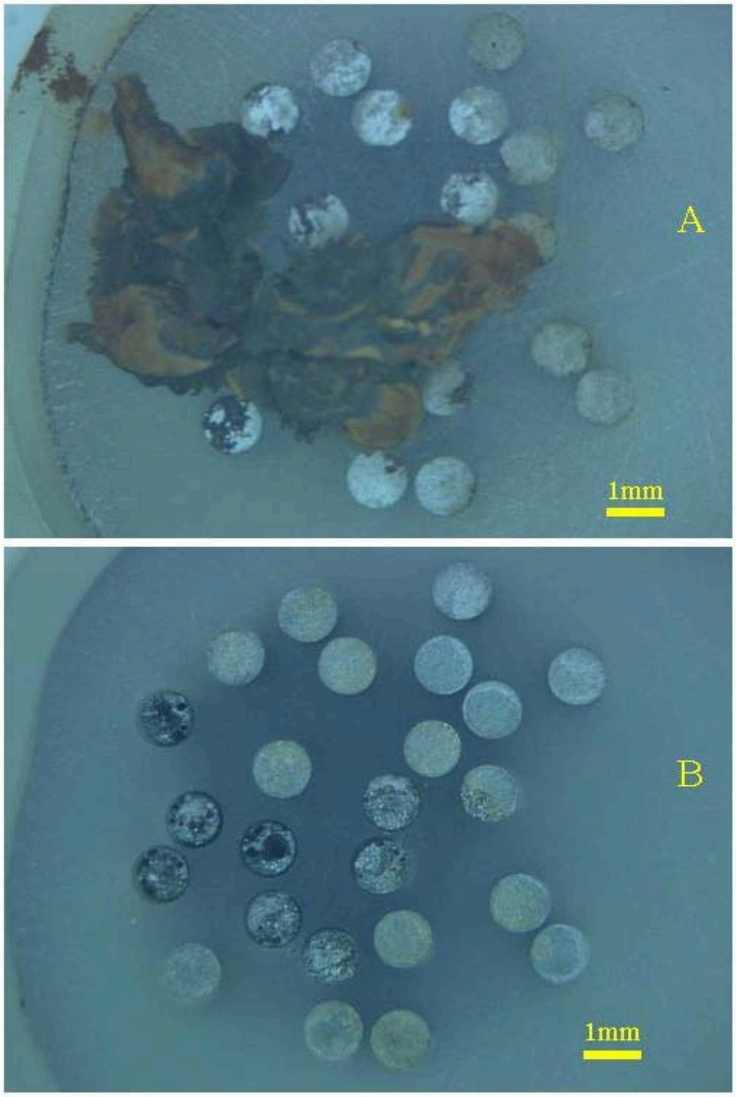

Figure 11: **Typical appearances of the sensor surface before (A) and after (B) removing the loose deposits after a short-term service in the cooling water system. Maximum thickness of the loose deposits was approximately 3 mm.**

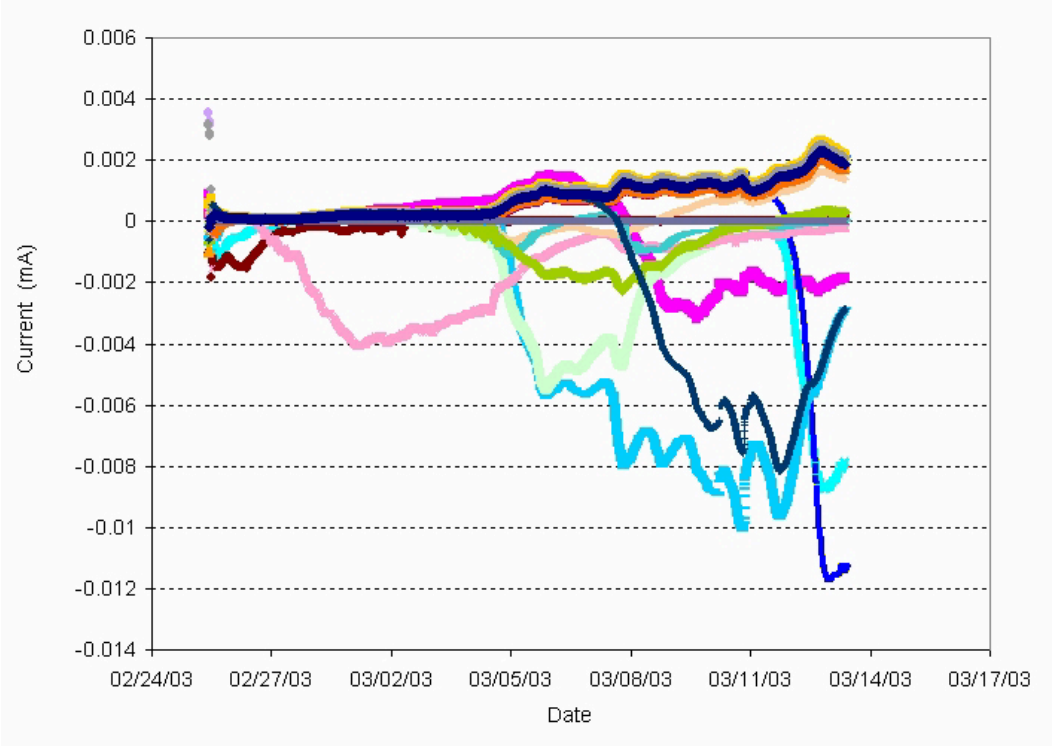

Figure 12: **Typical currents from the different sensing electrodes in a coupled multielectrode array sensor in the cooling water system during the monitoring period as shown in Figure 10. Note: The currents were from sensor CS-E5 in the makeup water**

Figure 13: **Field Corrosion Coupons after 1-month exposure in plant water. (Note that the areas outside of the under-deposit corroded locations still show the machining lines of the coupons from fabrication suggesting that once under-deposit corrosion initiated, corrosion propagated rapidly in these areas)**